

Distinguishing Nitro vs Nitrito Coordination in Cytochrome *c'* using Vibrational Spectroscopy and DFT.

Zach N. Nilsson,^{†||} Brian L. Mandella,[†] Kakali Sen,^{‡,⊥} Demet Kekilli,^{‡,#} Michael A. Hough,[‡] Pierre Moënne-Loccoz,^{*,§} Richard W. Strange,^{*,‡} Colin R. Andrew,^{*,†}

[†]Department of Chemistry and Biochemistry, Eastern Oregon University, La Grande, OR 97850

[‡]School of Biological Sciences, University of Essex, Colchester Essex, CO4 3SQ, UK

[⊥]Scientific Computing Department, STFC Daresbury Laboratory, Warrington, Cheshire, WA4 4AD, UK

[§]Division of Environmental and Biomolecular Systems, Oregon Health and Science University, Portland, OR 97239

ABSTRACT: Nitrite coordination to heme cofactors is a key step in the anaerobic production of the signaling molecule, nitric oxide (NO). An ambidentate ligand, nitrite has the potential to coordinate via the N- (nitro) or O- (nitrito) atoms in a manner that can direct its reactivity. Distinguishing nitro vs nitrito coordination, along with influence of the surrounding protein, is therefore of particular interest. In this study we probed Fe(III) heme-nitrite coordination in *Alcaligenes xylosoxidans* cytochrome *c'* (AXCP), an NO-carrier that excludes anions in its native state, but which readily binds nitrite ($K_d \sim 0.5$ mM) following a distal Leu16→Gly mutation to remove distal steric constraints. Room-temperature resonance Raman spectra (407 nm excitation) identify $\nu(\text{Fe}-\text{NO}_2)$, $\delta(\text{ONO})$, and $\nu_s(\text{NO}_2)$ nitrite ligand vibrations in solution. Illumination with 351 nm UV light results in photo-conversion to $\{\text{FeNO}\}^6$ and $\{\text{FeNO}\}^7$ states, enabling FTIR measurements to distinguish $\nu_s(\text{NO}_2)$ and $\nu_{as}(\text{NO}_2)$ vibrations from differential spectra. DFT calculations highlight the connections between heme environment, nitrite coordination mode, and vibrational properties, and confirm that nitrite binds to L16G AXCP exclusively through the N atom. Efforts to obtain the nitrite complex crystal structure were hampered by photochemistry in the X-ray beam. Although low dose crystal structures could be modelled with a mixed nitrite (nitro)/H₂O distal population, their photosensitivity and partial occupancy underscores the value of the vibrational approach. Overall, this study sheds light on steric determinants of heme-nitrite binding and provides vibrational benchmarks for future studies of heme protein nitrite reactions.

INTRODUCTION

Heme proteins are key players in metabolizing nitrite (NO_2^-) to the signaling molecule, nitric oxide (NO).¹ Nitrite binding to heme initiates the anaerobic production of NO in proteins such as hemoglobin (Hb), myoglobin (Mb), cytoglobin, neuroglobin, globin X (GbX), nitric oxide synthase, nitrophorins, and cytochrome *c* oxidases.¹⁻⁵ Within the nitrogen cycle, cytochrome *cd*₁ nitrite reductase also converts nitrite to NO during denitrification.⁶ Although the exact mechanisms of $\text{NO}_2^- \rightarrow \text{NO}$ conversion as a function of heme protein type (involving nitrite reductase, nitrite anhydrase, or nitrite dismutase activities) remain unresolved, each reaction begins with NO_2^- coordination to the heme Fe.

A characteristic of the nitrite anion is its ability to coordinate via its N-(nitro) or O-(nitrito) atoms (Figure 1). Since N- vs O- coordination is proposed to influence nitrite reactivity,⁶⁻⁹ establishing the particular Fe-nitrite coordination mode is an important first step in defining structure-reactivity relationships. Examples of $\eta_1\text{-N}$ and $\eta_1\text{-O}$ linkage isomerism have been reported in X-ray crystal structures of nitrite complexes of

Fe(III) heme proteins. N-atom nitro linkage is observed in crystal structures of heme-containing nitrite reductases^{10,11} and nitrophorins,^{12,13} whereas the nitrite complex of human hemoglobin (Hb)¹⁴ and chlorite dismutase¹⁵ exhibit O-atom *cis/trans*- and *cis*-nitrito modes, respectively. In the case of horse heart myoglobin (hh Mb), the nitrite coordination mode is sensitive to distal pocket mutations. Removal of distal H-bonding (H64V Mb) changed the nitrite coordination mode from an O-atom *trans*-nitrito (wt Mb) to N-bound nitro,⁸ while reinserting an H-bonding residue (H64V/V67R Mb) re-established O-atom coordination, albeit with a *cis*-like conformation.⁸

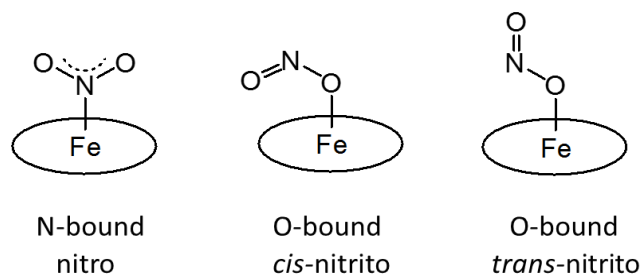


Figure 1. Heme-nitrite linkage isomers.

Theoretical studies predict that the energy differences between nitro and nitrito isomers of porphyrin complexes can range from $\sim 0 - 40 \text{ kJ mol}^{-1}$,^{7,9,16-20} and there are reports that the nitrite coordination mode can be affected by sample temperature as well as X-ray induced photochemistry.^{7, 21-23} Accordingly, there may be cases in which cryogenic crystal structures do not represent the nitrite coordination mode present under physiological conditions.

The most commonly applied spectroscopic techniques for studying heme-nitrite binding in solution (UV-vis and EPR) detect nitrite coordination indirectly via its effect on the Fe(III) spin state. However, the Fe(III) spin-state does not unambiguously define the nitrite linkage isomer. Ford and coworkers have reported examples of nitro and nitrito Fe-porphyrin complexes that are both low spin (LS) with indistinguishable UV-vis absorbance spectra.¹⁷ Moreover, the spin state can vary in response to sample temperature - a case in point being the Fe(III)nitrite complex of Mb, where cryogenic EPR spectra reveal a high spin (HS) complex, whereas room-temperature UV-vis spectra indicate a mixture of HS and LS species.²³

A direct means of spectroscopically probing heme-nitrite coordination is via the vibrational frequencies of the Fe-nitrite unit. Experimental frequencies (from RR or FTIR spectroscopy) can be compared with data from model complexes and DFT calculations to distinguish between different nitrite coordination modes. Heme-nitrite vibrations were recently reported for two protein complexes: Mb and horseradish peroxidase (HRP).²⁴⁻²⁷ However, in both cases, nitrite undergoes additional reactions with the porphyrin vinyl groups, altering the absorption, spin-state, and vibrational properties. By contrast, *c*-type cytochromes (in which porphyrin vinyl groups are replaced by thioether linkages) are not susceptible to nitrovinyl formation.

Cytochromes *c'* are NO-binding *c*-type heme proteins found in certain bacteria, including denitrifying, methanotrophic, nitrogen-fixing, and pathogenic organisms.²⁸ Despite containing mono-His ligated heme, their crowded hydrophobic distal pockets severely hinder coordination with exogenous ligands, even forcing NO to bind to the opposite (proximal) heme face.²⁹ Replacement of the distal Leu16 residue of *Alcaligenes xylosoxidans* cytochrome *c'* (AXCP) with Gly or Ala boosts the Fe(II) heme affinities for diatomic gas ligands by a remarkable $\sim 10^6 - 10^8$ -fold,²⁹⁻³¹ an effect ascribed to a more accessible distal site as well as ultra-efficient geminate recombination.³² In this study, we harnessed the favorable distal heme reactivity of L16G AXCP to characterize nitrite coordination to the Fe(III) state using spectroscopy (RR, FTIR, UV-visible absorption, and EPR), stopped-flow kinetics, DFT calculations, and X-ray crystallography. Ferric L16G AXCP has a nitrite affinity ($K_d \sim 0.5 \text{ mM}$) that is $\sim 20 - 30$ times greater than that of myoglobin, despite the absence of distal H-bonding. Vibrations of the Fe(III) nitrite complex were identified using RR and FTIR spectroscopies. In the case of FTIR measurements, assignment of heme-ligand vibrations was facilitated by photo-conversion of the nitrite complex to heme-nitrosyl species upon illumination with UV light. Vibrational frequencies and isotope shifts establish that nitrite binds to L16G AXCP via the N- (rather than O-atom) in solution, in agreement with the lowest energy structure from

DFT modeling. Nitro coordination was also observed in cryogenic crystal structures of the L16G AXCP nitrite complex, although accompanying X-ray induced photochemistry underscores the value of vibrational techniques. Overall, this study sheds light on steric determinants of nitrite binding to cytochrome *c'*, and highlights the ability of vibrational spectroscopy to differentiate nitro vs nitrito coordination under physiological conditions.

EXPERIMENTAL

Protein Samples, Crystallization and Reagents. The L16G variant of AXCP was expressed and purified as described previously.³⁰ Sodium nitrite, including isotopically labeled $\text{Na}^{15}\text{NO}_2$ (98% ^{15}N , 95% CP) and $\text{Na}^{15}\text{N}^{18}\text{O}_2$ (98% ^{15}N , 95% ^{18}O , 95% CP), was obtained from Sigma-Aldrich. All samples and reagents were prepared in pH 7.0 buffer containing 50 mM MOPS and 0.10 M NaCl. L16G-nitrite AXCP crystals were prepared from the isolated L16G-CO complex³⁰ which was oxidized by adding 200 mM (final concentration) of potassium ferricyanide and left at room temperature for 30 mins. The sample was run down a PD-10 column to separate the oxidant from the protein. The ferric state was confirmed by UV-vis measurement. Crystallization hanging drops for the L16G AXCP-nitrite complex were set using 20 mg/ml of protein co-crystallized with 50 mM sodium nitrite, 2.2 M ammonium sulphate and 0.1 M HEPES at pH 7.5. Crystals were transferred for several seconds into cryoprotectant solution (2.2 M ammonium sulfate, 0.1 M HEPES with 40% sucrose) and then stored in liquid nitrogen, in preparation for X-ray data collection.

Stopped-flow Kinetics. Kinetic measurements were conducted at 25.0 °C using an Applied Photophysics SX.18MV-R stopped-flow spectrophotometer (dead time $\sim 1 \text{ ms}$) housed within an anaerobic glove box (Vacuum Atmospheres Company). Rate constants for nitrite binding were determined by rapidly mixing solutions of ferric L16G AXCP with equal volumes of nitrite solution, and monitoring the formation of the nitrite complex with monochromatic light (415 nm) using a photomultiplier detector. Concentrations of nitrite (150 – 600 μM after mixing) were maintained in > 10 -fold excess over the heme binding sites ($\sim 4 \mu\text{M}$ heme after mixing) to ensure pseudo-first order conditions. Pseudo-first order rate constants, k_{obs} , determined from single exponential fits of time courses, are the average of 3–5 separate kinetic runs. The bimolecular rate constant for nitrite binding (k_{on}) was determined from the slope of plot of k_{obs} versus nitrite concentration, with the nitrite off-rate constant, k_{off} , as the y-intercept. Kinetic measurements conducted in air-saturated buffer gave rate constants similar to those obtained under anaerobic conditions. Illumination of the L16G nitrite complex with the white-light output of the stopped-flow Xe arc lamp resulted in absorption features characteristic of the $\{\text{FeNO}\}^6$ species, followed by conversion to the $\{\text{FeNO}\}^7$ species (200 s total illumination). The UV-light photosensitivity of the nitrite complex was used in FTIR measurements to facilitate the identification of heme-ligand vibrations (*vide infra*).

Spectroscopic Measurements. UV-vis absorption spectra of L16G AXCP solutions containing $\sim 5 \mu\text{M}$ protein (in heme) were measured using a Cary 60 scanning spectrophotometer. Resonance Raman (RR) measurements of L16G AXCP were conducted on solutions containing $\sim 200 \mu\text{M}$ (in heme). RR

spectra were recorded on a custom McPherson 2061/207 spectrograph (100- μm slit width) equipped with a Princeton Instruments liquid N_2 -cooled (LN1100PB) CCD detector. Spectral dispersal was achieved using a 0.67-m focal length and 2400 grooves/mm holographic grating, except for measurements of $\nu(\text{Fe}-\text{NO}_2)$ isotope-shifts for which a 3600 grooves/mm grating and 1.00-m focal length were used. An excitation wavelength of 406.7 nm was provided by a krypton ion laser and the Rayleigh line was attenuated using a long-pass filter (RazorEdge, Semrock). Room-temperature RR spectra were collected in a 90° scattering geometry using 7 mW laser power (at the sample) and a reciprocating translation stage. RR spectra of frozen solutions (maintained at 110 K with a liquid nitrogen cold finger) were collected in a $\sim 150^\circ$ backscattering geometry with 25 mW laser power at the sample. RR spectra were measured over periods of 3 – 16 min, using CCl_4 , indene, and aspirin standards to calibrate Raman shifts to an accuracy of $\pm 1 \text{ cm}^{-1}$.

FTIR measurements were conducted at room temperature on solutions of the L16G Fe(III) nitrite complex (2 mM in heme). A $\sim 20 \mu\text{L}$ drop of protein solution was loaded onto the center of a CaF_2 window (International Crystal Laboratories) and a second window was gently placed on top of the droplet to form a film with a $15\text{-}\mu\text{m}$ path length controlled by a Teflon spacer (International Crystal Laboratories). After confirming the integrity of the Fe(III) L16G-nitrite complex via UV-vis absorbance spectra, FTIR spectra were recorded on a Bruker Tensor 27 instrument equipped with a liquid N_2 -cooled MCT detector with sets of 1000-scan accumulations at 4-cm^{-1} resolution. The FTIR spectra were collected before and after illumination of the film directly inside the FTIR sample chamber with the 351-nm laser emission of a Krypton laser (Innova 302C, Coherent) for 16 min which resulted in the appearance of UV-vis absorption features consistent with the formation of $\{\text{FeNO}\}^6$ complex (λ_{max} 417, 533, 562 nm) and $\{\text{FeNO}\}^7$ (λ_{max} 416, 541, 574 nm) complexes. Comparison of “dark – illuminated” differential spectra obtained for different nitrite isotopomers enabled identification of Fe(III) nitrite vibrations as positive bands and nitrosyl vibrations as negative bands.

EPR spectra were recorded on a Bruker E-500 X-band EPR spectrometer equipped with a superX microwave bridge and a dual-mode cavity with a helium flow cryostat (ESR900, Oxford Instrument). The protein concentration was 100 μM and formation of the Fe(III) nitrite complex was confirmed by direct measurement of the visible spectrum in the EPR tube. Samples were frozen in liquid nitrogen and maintained at 10 K during the acquisition of the EPR spectra. The microwave frequency was 9.69 GHz, microwave power 2 mW, the modulation frequency 100 kHz, and the modulation amplitude 10 G.

Crystallographic Data Collection and Processing. Diffraction data to 1.06 \AA resolution were recorded on beamline I04-1 at the Diamond Light Source at 100 K, using a Pilatus 6M-F detector and X-ray wavelength 0.92 \AA . Images were processed using XDS³³ and Aimless³⁴ and the structure was refined and modelled using Refmac5³⁵ and Coot,³⁶ from a starting structure of the native L16G coordinates.³⁰ Processing and refinement statistics are given in Table S1.

DFT Calculations. These simulations were performed prior to the nitrite complex being obtained experimentally, using the crystal structure of L16G-CO AXCP (PDB 2yl3) as a template. The nitrite ligand was modelled at the distal position

to Fe(III) heme by coordination to either N or O. The *c*-heme was modeled as protoporphyrin IX including the propionate groups but discarding the covalently linked Cys residues. His 120 was included in the proximal position and the Met 19 residue was included along with Gly 16 to define the distal steric pocket, all residues being truncated at their $\text{C}\alpha$ atoms. The structures were optimized at DFT level using the B3LYP functional together with the DFT-D3 dispersion correction.³⁷ The def2-TZVP basis set was used for Fe(III) and def2-SVP³⁸ for all the other atoms. A ‘fragment optimization’ protocol within the ORCA package was used for the simulations:³⁹ the system was divided into several fragments corresponding to the active site residues and heme unit. These individual fragments were internally optimized and pair-wise constraints with respect to the distances and orientations between the amino acid fragments and the heme unit were applied during the optimization. The final structures were subjected to frequency calculations at the same level of theory, using natural $^{14}\text{N}^{16}\text{O}_2^-$ and the isotopes $^{15}\text{N}^{16}\text{O}_2^-$ and $^{15}\text{N}^{18}\text{O}_2^-$.

RESULTS

Ferric L16G AXCP and its reactivity with nitrite. In contrast to the ferric state of wt AXCP, which retains a 5c heme with no detectable binding of H_2O or anions,²⁸ the ferric L16G variant exhibits spectroscopic properties indicative of 6c heme with a distal water ligand. Solutions of ferric L16G AXCP (pH 7.0) exhibit a Soret absorption at 405 nm, with unresolved α/β bands at ~ 500 nm and a charge-transfer (CT) high-spin marker absorption at 627 nm (Figure 2, Table S2), while porphyrin marker RR vibrations obtained with 407 nm excitation have frequencies characteristic of 6cHS Fe(III) heme (Figure S1, Table S3). Addition of nitrite to ferric L16G AXCP generates a new set of absorbance bands (415, 536, and 569 nm) and porphyrin marker vibrations consistent with a 6cLS heme-nitrite complex (Figure 2, Tables S2 and S3).

Low-spin RR marker bands are retained upon cooling to 110 K (Figure S2). EPR spectra obtained at 10 K also indicate the presence of low-spin species with dominant g values consistent with histidine and N-based axial ligand ($g_x, g_y, g_z, 1.56, 2.36, 2.87$) (Figure S3).⁴⁰⁻⁴² The nitrite affinity of L16G AXCP, ($K_d = 0.50 \pm 0.15 \text{ mM}$ by titration) is comparable or higher than that of other ferric heme proteins such as Mb ($K_d \sim 17 \text{ mM}$) and Hb ($K_d \sim 3 \text{ mM}$) (Figure S4, Table S4). Stopped-flow measurements using monochromatic (415-nm) light yield rate constants for nitrite binding, k_{on} ($610 \pm 30 \text{ M}^{-1} \text{ s}^{-1}$) and nitrite release, k_{off} ($0.41 \pm 0.01 \text{ s}^{-1}$) (Figures S5 and S6), with a K_d value calculated from the $k_{\text{off}}/k_{\text{on}}$ ratio ($\sim 0.67 \text{ mM}$) in good agreement with titration measurements (Table S4).

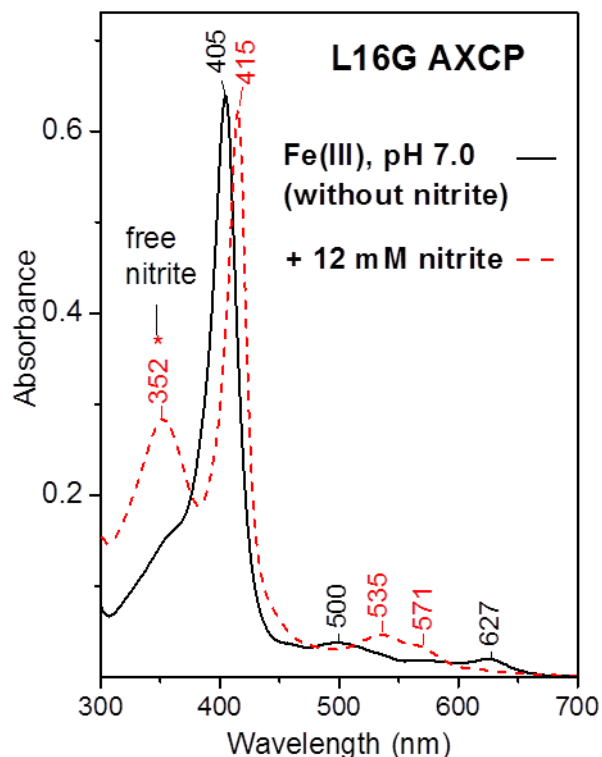


Figure 2. Effect of nitrite on the UV-visible absorption spectrum of Fe(III) L16G AXCP.

Identification of Fe(III)nitrite vibrations. Vibrations of the L16G Fe(III)NO₂⁻ unit were identified by RR and FTIR spectroscopy from their frequency downshifts in samples prepared with ¹⁵NO₂⁻ or ¹⁵N¹⁸O₂⁻. Specific vibrational assignments are supported by DFT calculations on energy-minimized structures (described later). RR measurements (407 nm excitation) detect three isotope-sensitive bands in the 300 – 1400 cm⁻¹ region (Figures 3 and S7). The RR band at 816 cm⁻¹ shifts by -7 cm⁻¹ (¹⁵NO₂⁻) and -40 cm⁻¹ (¹⁵N¹⁸O₂⁻), while the 1311 cm⁻¹ mode shifts by -21 cm⁻¹ (¹⁵NO₂⁻) and -57 cm⁻¹ (¹⁵N¹⁸O₂⁻) (Table 1). By comparison with FTIR frequencies of sublimed-solid Fe(III)porphyrin nitro complexes such as Fe(TTP)(NH₃)(NO₂),⁴¹ the 816-cm⁻¹ band is ascribed to nitrite ligand bending $\delta(\text{ONO})$, and the 1311-cm⁻¹ band to the nitrite ligand symmetric stretch, $\nu_s(\text{NO}_2)$ (Table 1).

An additional weak RR band observed in the present study at 308 cm⁻¹ that exhibits a -2 cm⁻¹ shift with ¹⁵N¹⁸O₂⁻, but no detectable shift with ¹⁵NO₂⁻ is suggestive of Fe-NO₂ stretching character, $\nu(\text{Fe-NO}_2)$ (Figure 4, Table 1). Cooling the RR samples to 110 K led to decreased signal quality that precluded the observation of the weaker nitrite ligand modes, although the ¹⁵NO₂⁻-sensitive $\delta(\text{ONO})$ mode is clearly visible at 815 cm⁻¹ (Figure S2). Finally, we note that RR spectra show no evidence of nitrite-derived heme-nitrosyl species, based on the absence of N-isotope shifts in the 400 – 600 cm⁻¹ region (Figure S7) that would indicate $\nu(\text{FeNO})$ vibrations.⁴⁴

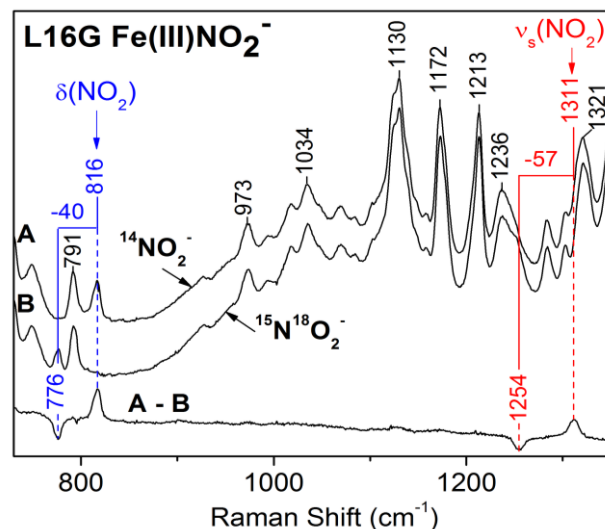


Figure 3. Mid-frequency RR region of ferric nitrite L16G AXCP showing the identification of $\delta(\text{NO}_2)$ and $\nu_s(\text{NO}_2)$ vibrations via substitution with ¹⁵N¹⁸O₂⁻.

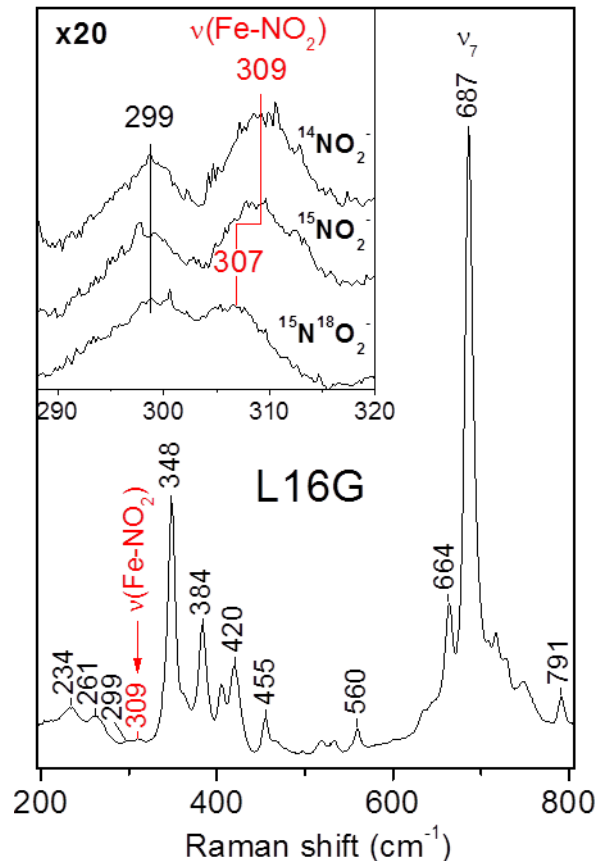


Figure 4. Low frequency RR spectrum of Fe(III)NO₂⁻ L16G AXCP. Inset shows the identification of the $\nu(\text{Fe-NO}_2)$ vibration via isotopic substitution. Isotope data for the ~400-800 cm⁻¹ region is shown in Figure S7).

Vibrational assignments complementary to those obtained from RR data were provided by differential FTIR measurements, using UV-light sensitivity of the L16G AXCP nitrite complex. Upon exposure to UV-light (Xe arc lamp or Kr laser 351 nm line), room-temperature solutions of the L16G nitrite complex exhibited spectroscopic changes consistent with the formation of Fe(III)- and Fe(II)-nitrosyl states (denoted $\{\text{FeNO}\}^6$ and $\{\text{FeNO}\}^7$, respectively, to indicate the sum of electrons in metal d and nitrosyl π^* orbitals). A comparison of optical spectra recorded during the photoreaction (Figure S8, bottom panel) with absorption maxima of independently-generated L16G AXCP heme species (Figure S8, top panel) suggest that the nitrite complex (415, 536, 569 nm) initially generates the $\{\text{FeNO}\}^6$ state (419, 530, 564 nm) which then converts to $\{\text{FeNO}\}^7$ (416, 541, 574 nm) (Figure S8). This photochemistry was confirmed and further monitored by FTIR spectroscopy. Accumulation of successive data before and after UV-irradiation generated room-temperature photolysis differential FTIR spectra, where vibrations from decaying species are observed as positive bands, while negative bands reflect new photo-generated species (Figure 5). A sharp band at 1313 cm^{-1} that decreases upon illumination of unlabeled L16G AXCP(NO_2^-) and that shifts by -21 cm^{-1} ($^{15}\text{NO}_2^-$) and -56 cm^{-1} ($^{15}\text{N}^{18}\text{O}_2^-$) is readily assigned to the $\nu_s(\text{NO}_2)$ mode of the L16G AXCP nitrite ligand observed at 1311 cm^{-1} in the RR (Table 1) (Figure 5). A weaker 1396 cm^{-1} FTIR band not identified in the RR spectra, shifts by -30 cm^{-1} ($^{15}\text{NO}_2^-$) and -62 cm^{-1} ($^{15}\text{N}^{18}\text{O}_2^-$), and is attributed to the asymmetric stretch of the nitrite ligand, $\nu_{as}(\text{NO}_2)$, in agreement with FTIR frequencies of inorganic Fe(III)porphyrin nitro complexes (Table 1).⁴³ Another broad feature at $\sim 1230\text{ cm}^{-1}$ that decreases upon illumination and that downshifts by $\sim 13\text{ cm}^{-1}$ ($^{15}\text{NO}_2^-$) and $\sim 54\text{ cm}^{-1}$ ($^{15}\text{N}^{18}\text{O}_2^-$) is consistent with the $\nu_{as}(\text{NO}_2)$ mode of free nitrite in aqueous solution (Table 1). In line with trends noted for inorganic nitro complexes,⁴⁴ the $\nu_{as}(\text{NO}_2)$ frequency of L16G AXCP(NO_2^-) (1396 cm^{-1}) is significantly higher than that of free nitrite ($\sim 1240\text{ cm}^{-1}$), whereas the $\nu_s(\text{NO}_2)$ frequencies of L16G AXCP(NO_2^-) (1313 cm^{-1}) and free nitrite are much closer.

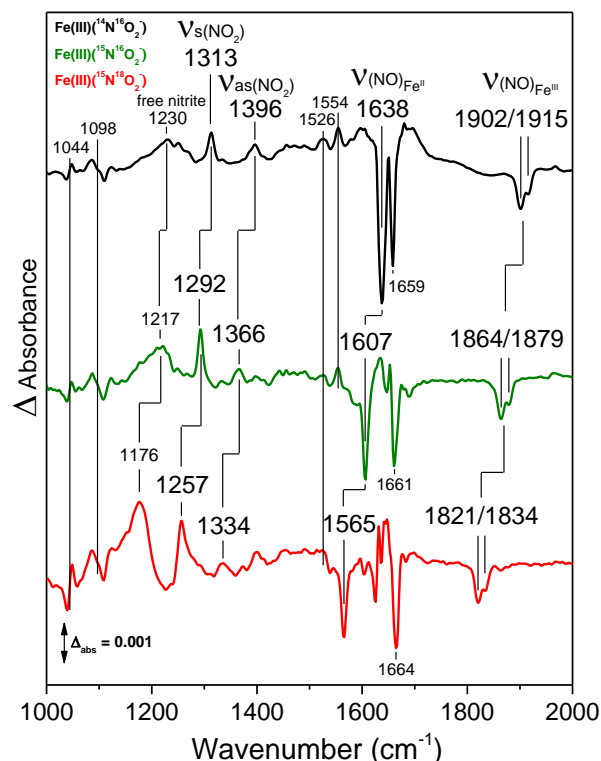
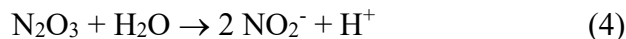


Figure 5. Room temperature FTIR difference spectra obtained after illumination of L16G Fe(III) nitrite complexes with 351 nm.

As counterpart to these decreasing FTIR signals, UV irradiation leads to the appearance of new modes consistent with $\nu(\text{NO})$ vibrations of heme $\{\text{FeNO}\}^6$ and $\{\text{FeNO}\}^7$ species. Specifically, a doublet peak at $1902/1915\text{ cm}^{-1}$ that downshifts by 37 cm^{-1} ($^{15}\text{NO}_2^-$) and 81 cm^{-1} ($^{15}\text{N}^{18}\text{O}_2^-$) is attributed to $\nu(\text{NO})$ modes of the $\{\text{FeNO}\}^6$ complex with minor conformational heterogeneity. In addition, an intense band at 1638 cm^{-1} which shifts by -31 cm^{-1} ($^{15}\text{NO}_2^-$) and -73 cm^{-1} ($^{15}\text{N}^{18}\text{O}_2^-$) (Figure 5) is assigned to the $\nu(\text{NO})$ mode of the heme $\{\text{FeNO}\}^7$ complex, in line with RR spectra of $\{\text{FeNO}\}^7$ L16G AXCP which show an isotope-sensitive $\nu(\text{NO})$ band at 1630 cm^{-1} shifting by -78 cm^{-1} with $^{15}\text{N}^{18}\text{O}$ (Figure S9). All other differential FTIR signals show no significant sensitivity to isotopic labelling of nitrite and are thus assigned to minor porphyrin and protein reorganization upon conversion of the ferric heme-nitro complex to the heme $\{\text{FeNO}\}^6$ and $\{\text{FeNO}\}^7$ species.

Because the reported photochemistry was not observed with visible light (Kr laser 407-nm and UV-free Xe arc lamp), and was also precluded in samples maintained at cryogenic temperatures, we propose that the conversion of the heme-nitrite complex to the $\{\text{FeNO}\}^6$ species depends on bimolecular reactions with photolysis products from free nitrite in solution. The photochemistry of nitrite in water upon excitation within its intense $n \rightarrow \pi^*$ transition at 354 nm ($\epsilon = 22.7\text{ M}^{-1}\text{ cm}^{-1}$) is well documented and known to produce NO and hydroxyl radicals.^{50,51} Rapid radical reactions with free nitrite typically lead to no net reaction (eqs 1–4), but in presence of L16G AXCP, photogenerated NO and NO_2 radicals may react to form the $\{\text{FeNO}\}^6$ species before further reduction to the $\{\text{FeNO}\}^7$ state

through additional photochemistry and/or reductive nitrosylation.



DFT calculations. The issue of nitro vs nitrito coordination in L16G AXCP was also investigated by DFT. Calculations were performed using the heme environment from the L16G-CO AXCP crystal structure (PDB code 2YL3) as a template and replacing CO with either N-bound or O-bound nitrite (Figure S10). The optimized geometries of both models (Figure 6A and B) are close to that of the starting crystal structure, with the N-coordinated nitrite being lower in energy than the O-bound by 31.5 kJ mol⁻¹ (for energies see Figure S10), in line with N-bound nitrite as the experimentally observed species (confirmed by RR spectroscopy).

Both N- and O-bound forms have their heme propionates oriented towards the distal side (resembling the starting crystal structure), and N-bound nitrite remained the preferred mode in alternative models with either one or both propionates flipped to the proximal side. The symmetrically-bound nitro ligand (Figure 6A) has a calculated Fe-N (nitro) distance of 1.94 Å and O-N-O angle of ~ 123°, with sufficient space in the distal pocket to bind to Fe without perturbing the M19 residue, which lies ~ 4.7 Å from the Fe. By contrast, the higher-energy nitrito complex (Figure 6B) acquires a monodentate *cis* Fe(ONO) orientation (Fe-O bond length ~ 1.9 Å, and O-N-O angle ~ 118°) that is more constrained in its position in the heme pocket, by both the M19 and G16 residues.

Vibrational modes of the DFT-optimized structures are shown in Figure S11, with frequencies summarized in Table 1. The N-bound model gives the best agreement with experimental data. Although the calculated vibrational frequencies for the nitro ligand are somewhat higher than experimental values, there is good agreement with the observed pattern of isotope shifts (Table 1). The predicted frequency and ¹⁵NO₂/¹⁵N¹⁸O₂ isotope shifts for the ν(Fe-NO₂) mode (309, ~ 0/-1 cm⁻¹) correspond well with observed values (318, ~ 0/-2 cm⁻¹) (Table 1). Similarly, for the δ(NO₂) vibration, the calculated frequency and isotope dependence (849, ~ 8/-43 cm⁻¹) agree well with experiment (816, ~ 7/-40 cm⁻¹), while calculated frequencies for ν_s(NO₂) (1428, -23/-65 cm⁻¹) and ν_{as}(NO₂) (1588, -31/-69 cm⁻¹) compare to observed values of (1311, -21/-57 cm⁻¹) and (1396, -30/-62 cm⁻¹), respectively (Table 1). By contrast, the O-bound model results in poorer agreement with experimental values (Table 1). Most strikingly, the predicted frequencies and ¹⁵NO₂/¹⁵N¹⁸O₂ isotope shifts for the nitrito stretching modes, ν(N=O) (1608, -20/-73 cm⁻¹) and ν(N-O) (1094, -22/-47 cm⁻¹) do not correspond well with either of the observed nitro ligand stretches

(*vide infra*), while predicted frequencies for bending mode, δ(ONO) (886, -4/-48 cm⁻¹) show a poorer match with experiment than δ(NO₂) from the nitro model (*vide infra*).

X-ray crystal structure of the L16G AXCP nitrite complex. Ferric state L16G crystals grown in the presence of nitrite were used for structure determination. High doses of X-rays (0.78 MGy) led to loss of bound nitrite and observation of ambiguous electron density in the distal heme pocket, consistent with reduction to the Fe(II) state where nitrite does not bind. Attenuation of the beam allowed us to determine a low-dose (0.16 MGy) crystallographic dataset at 1.06 Å resolution (Table S1), capturing the ferric state before full reduction of the heme site by the X-rays occurred. The tertiary structure was found to be identical (rmsd < 0.2 Å) to that of nitrite-free L16G AXCP,³⁰ while the electron density at the Fe-heme site showed that a ligand larger than water was present (the *Fo-Fc* omit map is shown in Figure S12).

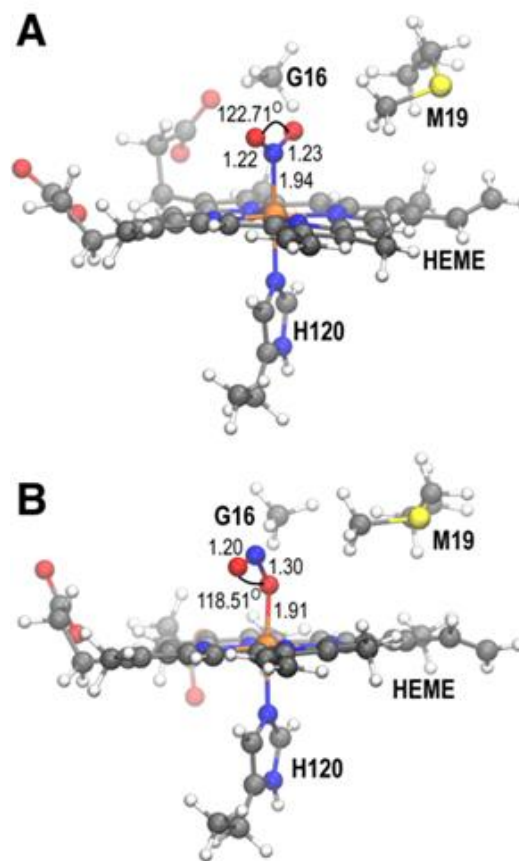


Figure 6. Optimized structures of the L16G AXCP Fe(III)nitrite complex showing (A) nitro and (B) nitrito coordination modes. Note: His120, Gly16, and Met19 residues are truncated at C α carbons as CH₃ groups.

Table 1. Vibrational frequencies (in cm^{-1}) of Fe(III) porphyrin nitrite complexes and other nitrite species.^a

nitrite species	$\nu_{\text{as}}(\text{NO}_2)$ or $\nu(N=O)$	$\nu_{\text{s}}(\text{NO}_2)$ or $\nu(N-O)$	$\delta(\text{NO}_2)$ or $\delta(ONO)$	$\nu(\text{Fe-NO}_2)$ or $\nu(\text{Fe-ONO})$	ref
6c nitro					
L16G AXCP (expt)	1396 (-30, -62)	1311 (-21, -57)	816 (-7, -40)	309 (~ 0, -2)	tw
L16G AXCP (calc)	1588 (-31, -69)	1428 (-23, -65)	849 (-8, -43)	318 (~ 0, -1)	tw
Fe(TTP)(1-MeIm)(NO ₂)	1396 (-33)	1312 (-21)	813 (-7)	nd	46
Fe(TTP)(NH ₃)(NO ₂)	1401 (-34)	1312 (-21)	810 (-6)	nd	46
Fe(TTP)(py)(NO ₂)	1405 (-32)	1306 (-19)	810 (-6)	nd	46
HRP	nd	1272 (-32, -54)	822 (-7, -44/-24)	563 (-19, -23)	27
6c nitrito					
Fe(TTP)(NH ₃)(ONO)	<i>1470 (-32)</i>	<i>969 (-17)</i>	<i>~ 827 (-5)</i>	nd	46
Mb	<i>1470 (-35, -70)</i>	<i>998 (-28, -44)</i>	<i>818 (-20, -28)</i>	<i>296/256 (0, -18)</i>	24,26
L16G AXCP (calc)	<i>1608 (-20, -73)</i>	<i>1094 (-22, -47)</i>	<i>886 (-4, -48)</i>	<i>328 (~ 0, -2)</i>	tw
5c nitrito					
Fe(TTP)(ONO)	<i>1528 (-34)</i>	<i>902 (-23)</i>	<i>751 (-4)</i>	nd	47
nitrovinyl					
HRP	nd	1334 (-25, -55)	nd	-	27
Mb	1518 (-36)	1324 (-20)	nd	-	24,26
free nitrite					
NO ₂ ⁻ (aq)	~1240	1325-1331	817	-	50,51

^a Data in italics refer to nitrito vibrations. Values in parentheses indicate frequency shifts upon substitution with ¹⁵NO₂⁻ and ¹⁵N¹⁸O₂⁻. Abbreviations: tw, this work; nd, not determined.

The atomic resolution of the data allowed us to successfully model a mixture of a nitro-coordinated nitrite with Fe-N distance 2.1 Å and a water molecule at 2.07 Å (Figure 7), in the proportion ~ 1:3. The Fe-N(His) distance is 2.04 Å. The nitrite is located in the distal heme pocket with its O1 atom oriented towards and 3.3 Å away from the Met19Sδ atom and 3.1 Å from the Gly16Cα atom. Measurement of datasets with higher X-ray doses revealed gradual loss of the nitrite ligand and a structure best modelled by a single water molecule coordinated to Fe(II) heme at 2.08 Å, with Fe-N(His) at 2.07 Å. While unusual, it is noted that a putative Fe(II)-OH₂ complex (Fe-O distance of 2.17 Å) was recently reported for the chemically-reduced state of the L16A variant of AXCP.²⁹ Although we were able to model N-bound (nitro) coordination in low-dose structures (in agreement with our vibrational and DFT data), the X-ray sensitivity of the Fe(III) nitrite-bound crystals highlights the need for structural characterization using alternate (vibrational) techniques (*vide supra*).

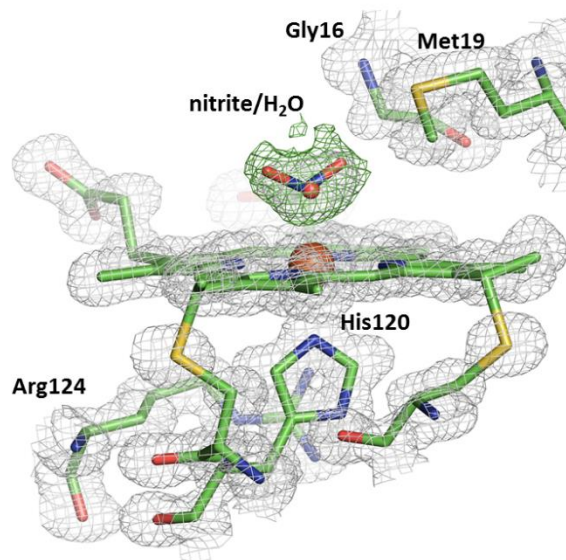


Figure 7. Low dose (0.16 MGy) X-ray crystal structure of the heme environment of L16G-nitrite AXCP at 1.06 Å resolution showing a weighted electron density *Fo-Fc* omit map (green) superimposed on the *2Fo-Fc* map (grey), contoured at 0.44 e/Å³. A mixture of nitrite and water were modelled as heme ligands in the proportion 0.25:0.75 to account for the ligand electron density, with B-factors 19.6/17.8/19.7 Å² for nitrite O/N/O atoms, 10.4 Å² for water and 8.9 Å² for the Fe atom. The Fe-N(nitrite) distance is 2.1 Å, Fe-N-O angles 118°/120° and Fe-water distance 2.07 Å.

DISCUSSION

Vibrational identification of nitro coordination. We report the first vibrational and DFT analysis of a *c*-type heme protein nitrite complex. Observed vibrational frequencies for the L16G AXCP Fe(III)NO₂⁻ unit are in excellent agreement with previous FTIR data for Fe(III)porphyrin nitro complexes with nitrogenous base proximal ligands (Table 1).⁴⁶ Defining frequencies of these heme-nitro complexes include: $\nu_{\text{as}}(\text{NO}_2) \sim 1395 - 1406 \text{ cm}^{-1}$, $\nu_{\text{s}}(\text{NO}_2) \sim 1306 - 1312 \text{ cm}^{-1}$, and $\delta(\text{NO}_2) \sim 810 - 816 \text{ cm}^{-1}$. RR spectra of L16G AXCP also identify the $\nu(\text{Fe}-\text{NO}_2)$ vibration at 309 cm^{-1} . Vibrational assignments are supported by DFT calculations on L16G AXCP which, despite overestimating the absolute frequencies, reproduce the ¹⁵N¹⁶O₂⁻ and ¹⁵N¹⁸O₂⁻ isotope shifts quite well.

In contrast to nitro complexes, monodentate nitrito complexes breaks the conjugation of the N–O bonds, leading to one N–O stretch at higher energy (corresponding at an N=O double bond) and another N–O stretch at lower energy (corresponding to an N–O single bond). Such behavior has been previously reported for complexes of Co(III) and Cr(III),^{45,52} as well as for Cu(II)(tris(pyrazolyl)methane)⁵³ and Fe(III)(TTP)(NH₃).⁴⁶ In the latter case, the nitrito isomer is clearly distinguished from its nitro isomer by the existence of an $\nu(\text{N}=\text{O})$ mode at 1470 cm^{-1} (higher than the $\nu_{\text{as}}(\text{NO}_2)$ nitro frequency), and an $\nu(\text{N}-\text{O})$ mode at 969 cm^{-1} (lower than the nitro $\nu_{\text{s}}(\text{NO}_2)$ frequency) (Table 1). The nitrito ligand bending frequency ($\sim 827 \text{ cm}^{-1}$) is also slightly higher than that of the nitro counterpart ($\sim 810 \text{ cm}^{-1}$). Our DFT calculations on N-bound vs O-bound models for L16G AXCP reveal the same distinguishing vibrational trends as described above (albeit with higher absolute frequencies), while also predicting that the $\nu(\text{Fe}-\text{ONO})$ frequency is slightly higher than that of the nitro isomer $\nu(\text{Fe}-\text{NO}_2)$ mode (Table 1).

To our knowledge, the present RR and FTIR data for L16G AXCP contain the first vibrational frequencies of nitrite bound to an Fe(III) heme protein without accompanying porphyrin (vinyl) nitration. Very recently, RR spectra were reported for Fe(III) Mb²⁴⁻²⁶ and HRP²⁷ incubated for extended periods with nitrite. It has been shown that these conditions lead to nitration of the porphyrin 2-vinyl group (Mb) or the 4-vinyl group (HRP).^{54,55} This so-called “nitriheme” is the basis of the green-coloration in cured meat upon prolonged exposure to excess nitrite under acidic conditions. Mb incubated with 50 mM nitrite leads to the formation of a 6cHS Fe(III) heme nitrito complex ($\lambda_{\text{max}} 410 \text{ nm}$), and upon prolonged incubation, to a 6cLS heme nitrito/nitrovinyl complex ($\lambda_{\text{max}} 450 \text{ nm}$).^{24,25} Consistent with nitrito coordination, RR spectra of Mb nitrite complex identified an $\nu(\text{N}=\text{O})$ frequency (1470 cm^{-1})²⁶ although bands assigned to $\nu(\text{N}-\text{O})$ and $\delta(\text{ONO})$ exhibited somewhat different frequencies and/or isotope shifts compared to Fe(TTP)(NH₃)(ONO) (Table 1).

In the case of Fe(III) HRP,²⁷ incubation with 50 mM nitrite at pH 7.5 for 3 h led to the generation of a nitrovinyl porphyrin species with a $\nu_{\text{s}}(\text{NO}_2)$ RR band at 1334 cm^{-1} but no nitrite coordination to the heme Fe. Upon lowering the pH to 5.5, additional RR frequencies consistent with a low spin Fe(III) heme complex were observed, including several vibrations assigned to a heme-bound nitro complex. The $\nu_{\text{s}}(\text{NO}_2)$ of Fe(III)nitro HRP was assigned at 1272 cm^{-1} on the basis of its isotope shifts

with ¹⁵N¹⁶O₂⁻ (-32 cm^{-1}) and ¹⁵N¹⁸O₂⁻ (-54 cm^{-1}). Two other bands at 822 and 563 cm^{-1} were assigned to $\delta(\text{NO}_2)$ and $\nu(\text{Fe}-\text{NO}_2)$, respectively, based on their nitrite-isotope sensitivity. Although the $\delta(\text{NO}_2)$ mode of HRP (822 cm^{-1}) corresponds well to that of Fe(III)NO₂⁻ L16G AXCP (816 cm^{-1}) (including similar isotope-dependence), other vibrations are quite different (Table 1). In particular, the $\nu_{\text{s}}(\text{NO}_2)$ mode of HRP (1272 cm^{-1}) is 39 cm^{-1} lower than that of L16G AXCP, while the purported $\nu(\text{Fe}-\text{NO}_2)$ frequency of HRP (563 cm^{-1}) is significantly higher than that of L16G AXCP (309 cm^{-1}) and exhibits much larger ¹⁵N¹⁶O₂⁻/¹⁵N¹⁸O₂⁻ isotope shifts ($-19/-23 \text{ cm}^{-1}$) than those of L16G AXCP ($\sim 0/-2 \text{ cm}^{-1}$). While the origin of these discrepancies is unclear, they highlight the need for reliable benchmark frequencies for heme-nitrite complexes. *Determinants and consequences of nitro vs nitrito coordination.* The present study highlights the role of steric factors in controlling heme protein nitrite interactions. Native AXCP has a sterically crowded and hydrophobic distal pocket which limits exogenous ligand binding to weakly-bound CO and NO complexes. Removal of steric hindrance via the Leu16 → Gly mutation not only dramatically boosts the affinity for diatomic gases,^{29,30} it also expands the repertoire of accessible ligands to include the triatomic NO₂⁻ anion. Our DFT calculations on L16G AXCP predict that N-bound nitrite is energetically favored over O-bound, with additional N- vs O- selectivity possibly arising from steric interactions with Met19.

There appears to be some connection between H-bond stabilization and the nitrite coordination mode. A common feature of heme proteins that exhibit O-bound nitrite (Mb, Hb, chlorite dismutase) is the presence of distal pocket H-bond donors. It is possible that distal H-bonding to nitrite lowers $k_{\text{off}}(\text{NO}_2^-)$, and that this is reflected in a relatively low $k_{\text{off}}(\text{NO}_2^-)/k_{\text{off}}(\text{CO})$ ratio (since heme-CO complexes are not stabilized significantly by H-bonding).⁵⁶ Indeed, the $k_{\text{off}}(\text{NO}_2^-)/k_{\text{off}}(\text{CO})$ ratio for Mb (~ 140) is ~ 400 -fold lower than for L16G AXCP ($\sim 5.5 \times 10^4$) (which lacks distal H-bonding residues). Nevertheless, the present study underscores the need for nitro vs nitrito coordination to also be taken into account when interpreting heme-nitrite reactivity trends.

SUMMARY

Using vibrational spectroscopy (RR and FTIR), DFT calculations, and X-ray crystallography we show that a distal pocket L16G variant of cytochrome *c*' coordinates nitrite via an N-bound (nitro) mode across a range of sample conditions. In particular, the present study highlights the importance of vibrational spectroscopy in distinguishing N- vs O-bound nitrite under physiological conditions, providing a foundation for future characterization of biological heme-nitrite chemistry.

ASSOCIATED CONTENT

Supporting Information.

Experimental details; additional spectroscopic, kinetic, DFT, and structural data (PDF). The supporting information is available free of charge on the ACS Publications website at <http://pubs.acs.org>.

AUTHOR INFORMATION

Corresponding Authors

*rstrange@essex.ac.uk

*moennelo@ohsu.edu

*candrew@eou.edu

Present Addresses

^{||} Chemistry Department, Colorado State University, Ft. Collins, CO 80523

[#] Department of Biology and Chemistry, Paul Scherer Institute, CH-5232 Villigen PSI, Switzerland

ORCID

Richard W. Strange: 0000-0001-8825-3608

Pierre Moënnelocoz: 0000-0002-76847617

Colin R. Andrew: 0000-0001-5908-012X

Notes

The authors declare no competing financial interest.

ACKNOWLEDGMENTS

This work was supported by the National Science Foundation (MCB-1411963 grant to C.R.A.), BBSRC (award BB/M020924/1 to R.W.S., supporting K.S.), the National Institutes of Health (GM74785 to P.M.-L.), and the Leverhulme Trust (Project Grant RPG2014-355 to M.H., supporting D.K.). The authors thank McKenzie Evans for help with initial experiments. We thank the Molecular Biophysics Group at the University of Liverpool UK for protocols for preparing the L16G variant.

REFERENCES

- (1) Kim-Shapiro, D. B.; Gladwin, M. T. Mechanisms of nitrite bioactivation. *Nitric Oxide* **2014**, *38*, 58–68.
- (2) Li, H.; Hemann, C.; Abdelghany, T. M.; El-Mahdy, M.; Zweier, J. L., Characterization of the mechanism and magnitude of cytoglobin-mediated nitrite reduction and nitric oxide generation under anaerobic conditions. *J. Biol. Chem.* **2012**, *287*, 36623–36633.
- (3) Petersen, M. G.; Dewilde, S.; Fago, A., Reactions of ferrous neuroglobin and cytoglobin with nitrite under anaerobic conditions. *J. Inorg. Biochem.* **2008**, *102*, 1777–1782.
- (4) Corti, P.; Xue, J.; Tejero, J.; Wajih, N.; Sun, M.; Stolz, D. B.; Tsang, M.; Kim-Shapiro, D. B.; Gladwin, M. T., Globin X is a six-coordinate globin that reduces nitrite to nitric oxide in fish red blood cells. *Proc. Natl. Acad. Sci. U. S. A.* **2016**, *113*, 8538–8543.
- (5) Loullis, A.; Noor, M. R.; Soulimane, T.; Pinakoulaki, E., The structure of a ferrous heme-nitro species in the binuclear heme a₃/CuB center of ba₃-cytochrome c oxidase as determined by resonance Raman spectroscopy. *Chem. Commun.*, **2015**, *51*, 286–289.
- (6) Averill, B. A., Dissimilatory nitrite and nitric oxide reductases. *Chem. Rev.* **1996**, *96*, 2951–2964.
- (7) Silaghi-Dumitrescu, R., Linkage isomerism in nitrite reduction by cytochrome cd₁ nitrite reductase. *Inorg. Chem.* **2004**, *43*, 3715–3718.
- (8) Yi, J.; Heinecke, J.; Tan, H.; Ford, P. C.; Richter-Addo, G. B., The distal pocket histidine residue in horse heart myoglobin directs the O-binding mode of nitrite to the heme iron. *J. Am. Chem. Soc.* **2009**, *131*, 18119–18128.
- (9) Berto, T. C.; Lehnert, N., Density functional theory modeling of the proposed nitrite anhydrase function of hemoglobin in hypoxia sensing. *Inorg. Chem.* **2011**, *50*, 7261–7363.
- (10) Williams, P. A.; V., F.; Garman, E. F.; Saunders, N. F. W.; Ferguson, S. J.; Hajdu, J., Haem-ligand switching during catalysis in crystals of a nitrogen-cycle enzyme. *Nature* **1997**, *389*, 406–412.
- (11) Lukat, P.; Rudolf, M.; Stach, P.; Messerschmidt, A.; Kron-eck, P. M. H.; Simon, J.; Einsle, O., Binding and reduction of sulfite by cytochrome c nitrite reductase. *Biochemistry* **2008**, *47*, 2080–2086.
- (12) He, C.; Ogata, H.; Knipp, M., Formation of the complex of nitrite with the ferriheme b beta-barrel proteins nitrophorin 4 and nitrophorin 7. *Biochemistry* **2010**, *49*, 5841–5851.
- (13) He, C.; Ogata, H.; Knipp, M., Insertion of an H-bonding residue into the distal pocket of the ferriheme protein nitrophorin 4: effect on nitrite-iron coordination and nitrite disproportionation. *Chem. Bio-divers.* **2012**, *9*, 1761–1775.
- (14) Yi, J.; Safo, M. K.; Richter-Addo, G. B., The nitrite anion binds to human hemoglobin via the uncommon O-nitrito mode. *Biochemistry* **2008**, *47*, 8247–8249.
- (15) Goblirsch, B. R.; Streit, B. R.; DuBois, J. L.; Wilmot, C. M., Structural features promoting dioxygen production by *Dechloromonas aromatica* chlorite dismutase. *J. Biol. Inorg. Chem.* **2010**, *15*, 879–888.
- (16) Novozhilova, I. V.; Coppens, P.; Lee, J.; Richter-Addo, G. B.; Bagley, K. A., Experimental and density functional theoretical investigations of linkage isomerism in six-coordinate {FeNO}⁶ iron porphyrins with axial nitrosyl and nitro ligands. *J. Am. Chem. Soc.* **2006**, *128*, 2093–2104.
- (17) Kurtikyan, T. S.; Hovhannisyan, A. A.; Hakobyan, M. E.; Patterson, J. C.; Iretskii, A.; Ford, P. C., Reactions of nitrogen oxides with five-coordinate Fe^{III}(porphyrin) nitrito intermediate Fe(Por)(ONO) in sublimed solids. *J. Am. Chem. Soc.* **2007**, *129*, 3576–3585.
- (18) Perissinotti, L. L.; Marti, M. A.; Doctorovich, F.; Luque, F. J.; Esterin, D. A., A microscopic study of the deoxyhemoglobin-catalyzed generation of nitric oxide from nitrite anion. *Biochemistry* **2008**, *47*, 9793–9802.
- (19) Hopmann, K. H.; Cardey, B.; Gladwin, M. T.; Kim-Shapiro, D. B.; Ghosh, A., Hemoglobin as a nitrite anhydrase: modeling methemoglobin-mediated N₂O₃ formation. *Chem. Eur. J.* **2011**, *17*, 6348–6358.
- (20) Xu, N.; Yi, J.; Richter-Addo, G. B., Linkage isomerization in heme-NO_x compounds: understanding NO, nitrite, and hyponitrite interactions with iron porphyrins. *Inorg. Chem.* **2010**, *49*, 6253–6266.
- (21) Trofimov, A. A.; Polyakov, K. M.; Boyko, K. M.; Tikhonova, T. V.; Safonova, T. N.; Tikhonov, A. V.; Popov, A. N.; Popov, V. O., Structures of complexes of octahaem cytochrome c nitrite reductase from *Thioalkalivibrio nitratireducens* with sulfite and cyanide. *Acta Crystallogr. D Biol. Crystallogr.* **2010**, *66*, 1043–1047.
- (22) Yi, J.; Orville, A. M.; Skinner, J. M.; Skinner, M. J.; Richter-Addo, G. B., Synchrotron X-ray-induced photoreduction of ferric myoglobin nitrite crystals gives the ferrous derivative with retention of the O-bonded nitrite ligand. *Biochemistry* **2010**, *49*, 5969–5971.
- (23) Silaghi-Dumitrescu, R.; Svistunenko, D. A.; Cioloboc, D.; Bischin, C.; Scurtu, F.; Cooper, C. E., Nitrite binding to globins: linkage isomerism, EPR silence and reductive chemistry. *Nitric Oxide* **2014**, *42*, 32–39.
- (24) Lambrou, A.; Pinakoulaki, E., Resonance Raman detection of the myoglobin nitrito heme Fe-O-N=O/2-nitrovinyl species: implications for helix E-helix F interactions. *Phys. Chem. Chem. Phys.* **2015**, *17*, 3841–3849.
- (25) Lambrou, A.; Ionno, A.; Pinakoulaki, E., Spin crossover in nitrito-myoglobin as revealed by resonance Raman spectroscopy. *Chem. Eur. J.* **2016**, *22*, 12176–12180.
- (26) Ioannou, A.; Lambrou, A.; Daskalakis, V.; Pinakoulaki, E., Nitrite coordination in myoglobin. *J. Inorg. Biochem.* **2017**, *166*, 49–54.
- (27) Ioannou, A.; Pinakoulaki, E., Probing nitrite coordination in horseradish peroxidase by resonance Raman spectroscopy: Detection of two binding sites. *J. Inorg. Biochem.* **2017**, *169*, 79–85.

- (28) Hough, M. A.; Andrew, C. R., Cytochromes *c'*: Structure, reactivity and relevance to haem-based gas sensing. *Adv. Microb. Physiol.* **2015**, *67*, 1–84.
- (29) Kekilli, D.; Petersen, C. A.; Pixton, D. A.; Ghafoor, D. D.; Abdullah, G. H.; Dworkowski, F. S. N.; Wilson, M. T.; Heyes, D. J.; Hardman, S. J. O.; Murphy, L. M.; Strange, R. W.; Scrutton, N. S.; Andrew, C. R.; Hough, M. A., Engineering proximal vs. distal heme–NO coordination via dinitrosyl dynamics: implications for NO sensor design. *Chem. Sci.* **2017**, *8*, 1986–1994.
- (30) Antonyuk, S. V.; Rustage, N.; Petersen, C. A.; Arnst, J. L.; Heyes, D. J.; Sharma, R.; Berry, N. G.; Scrutton, N. S.; Eady, R. R.; Andrew, C. R.; Hasnain, S. S., Carbon monoxide poisoning is prevented by the energy costs of conformational changes in gas-binding haemproteins. *Proc. Natl. Acad. Sci. U. S. A.* **2011**, *108*, 15780–15785.
- (31) Garton, E. M.; Pixton, D. A.; Petersen, C. A.; Eady, R. R.; S., H. S.; Andrew, C. R., A distal pocket Leu residue inhibits the binding of O₂ and NO at the distal heme site of cytochrome *c'*. *J. Am. Chem. Soc.* **2012**, *134*, 1461–1463.
- (32) Andrew, C. R.; Petrova, O. N.; Lamarre, I.; Lambry, J. C.; Rappaport, F.; Negerie, M., The dynamics behind the affinity: controlling heme-gas affinity via geminate recombination and heme propionate conformation in the NO-carrier cytochrome *c'*. *ACS Chem. Biol.* **2016**, *11*, 3191–3201.
- (33) Kabsch, W., Xds. *Acta Crystallogr. D Biol. Crystallogr.* **2010**, *66*, 125–132.
- (34) Evans, P. R.; Murshudov, G. N., How good are my data and what is the resolution? *Acta Crystallogr. D Biol. Crystallogr.* **2013**, *69*, 1204–1214.
- (35) Murshudov, G. N.; Skubák, P.; Lebedev, A. A.; Pannu, N. S.; Steiner, R. A.; Nicholls, R. A.; Winn, M. D.; Long, F.; Vagin, A. A., REFMAC5 for the refinement of macromolecular crystal structures. *Acta Crystallogr. D Biol. Crystallogr.* **2011**, *67*, 355–367.
- (36) Emsley, P.; Lohkamp, B.; Scott, W. G.; Cowtan, K., Features and development of Coot. *Acta Crystallogr. D Biol. Crystallogr.* **2010**, *66*, 486–501.
- (37) Grimme, S.; Antony, J.; Ehrlich, S.; Krieg, H., A consistent and accurate ab initio parametrization of density functional dispersion correction (DFT-D) for the 94 elements H–Pu. *J. Chem. Phys.* **2010**, *132*, 154104.
- (38) Weigend, F.; Ahlrichs, R., Balanced basis sets of split valence, triple zeta valence and quadruple zeta valence quality for H to Rn: Design and assessment of accuracy. *Phys. Chem. Chem. Phys.* **2005**, *7*, 3297–3305.
- (39) Neese, F., The ORCA program system. *WIREs Comput. Mol. Sci.* **2012**, *2*, 73–78.
- (40) Blumberg, W. E.; Peisach, J., The low-spin compounds of heme proteins. *Adv. Chem. Ser.* **1971**, *100*, 271–291.
- (41) Taylor, C. P., The EPR of low-spin heme complexes. Relation of the t_{2g} hole model to the directional properties of the g tensor, and a new method for calculating the ligand field parameters. *Biochim. Biophys. Acta.* **1977**, *491*, 137–148.
- (42) Young, L. J.; Siegel, L. M., On the reaction of ferric heme proteins with nitrite and sulfite. *Biochemistry* **1988**, *27*, 2790–2800.
- (43) Kurtikyan, T. S.; Ford, P. C., FTIR and optical spectroscopic studies of the reactions of heme models with nitric oxide and other NOx in porous layered solids. *Coord. Chem. Rev.* **2008**, *252*, 1486–1496.
- (44) Lehnert, N.; Scheidt, W. R.; Wolf, M. W., Structure and bonding in heme-nitrosyl complexes and implications for biology. *Struct. Bond.* **2014**, *154*, 155–224.
- (45) Nakamoto, K., *Infrared and Raman Spectra of Inorganic and Coordination Compounds*, part B, sixth edition, chapter 1 J. Wiley and Sons: New York, **2009**.
- (46) Kurtikyan, T. S.; Hovhannisyanyan, A. A.; Gulyan, G. M.; Ford, P. C., Interaction of nitrogen bases with iron-porphyrin nitrito complexes Fe(Por)(ONO) in sublimed solids. *Inorg. Chem.* **2007**, *46*, 7024–7031.
- (47) Kurtikyan, T. S.; Ford, P. C., Reactions of nitrogen oxides with heme models: spectral characterization of an elusive five-coordinate FeIII(porphyrin) nitrito intermediate. *Angew. Chem. Int. Ed. Eng.* **2006**, *45*, 492–496.
- (48) Irish, D. E.; Thorpe, R. V., Raman spectral studies of cadmium-nitrite interactions in aqueous solutions and crystals. *Can. J. Chem.* **1975**, *53*, 1414–1423.
- (49) Ianoul, A.; Coleman, T.; Asher, S. A., UV resonance Raman spectroscopic detection of nitrate and nitrite in wastewater treatment processes. *Anal. Chem.* **2002**, *74*, 1458–1461.
- (50) Zafiriou, O. C.; Bonneau, R., Wavelength-dependent quantum yield of OH radical formation from photolysis of nitrite ion in water. *Photochem. Photobiol.* **1987**, *45*, 723–727.
- (51) Jankowski, J. J.; Kieber, D. J.; Mopper, K., Nitrate and nitrite ultraviolet actinometers. *Photochem. Photobiol.* **1999**, *70*, 319–328.
- (52) Nakamoto, K.; Fujita, J.; Murata, H., Infrared spectra of metallic complexes. V. The infrared spectra of nitro and nitrito complexes. *J. Am. Chem. Soc.* **1958**, *80*, 4817–4823.
- (53) Lehnert, N.; Coornelissen, U.; Neese, F.; Ono, T.; Noguchi, Y.; Okamoto, K.; Fujisawa, K., Synthesis and spectroscopic characterization of copper(II)-nitrito complexes with hydrotris(pyrazoyl)borate and related coligands. *Inorg. Chem.* **2007**, *46*, 3916–3933.
- (54) Yi, J.; Richter-Addo, G. B., Unveiling the three-dimensional structure of the green pigment of nitrite-cured meat. *Chem. Commun.* **2012**, *48*, 4172–4174.
- (55) Wojciechowski, G.; Ortiz de Montellano, P. R., Radical energies and the regiochemistry of addition to heme groups. Methylperoxy and nitrite radical additions to the heme of horseradish peroxidase. *J. Am. Chem. Soc.* **2007**, *129*, 1663–1672.
- (56) Olson, J. S.; Phillips Jr., G. N., Myoglobin discriminates between O₂, NO and CO by electrostatic interactions with the bound ligand. *J. Biol. Inorg. Chem.* **1997**, *2*, 544–552.

Vibrational spectroscopy (Resonance Raman, FTIR), DFT calculations, and X-ray crystallography establish that a distal heme pocket variant of cytochrome *c'* coordinates nitrite via an N-bound (nitro) mode. Importantly, the vibrational approach distinguishes N- vs O-bound nitrite in room temperature solutions, with observed frequencies of the heme nitro complex ($\nu(\text{Fe}-\text{NO}_2) \sim 309 \text{ cm}^{-1}$, $\delta(\text{ONO}) \sim 816 \text{ cm}^{-1}$, $\nu_s(\text{NO}_2) \sim 1311 \text{ cm}^{-1}$, $\nu_{as}(\text{NO}_2) \sim 1396 \text{ cm}^{-1}$) providing useful benchmarks for future mechanistic studies of biological heme-nitrite chemistry.

For Table of Contents only.

